GaN-based Deep-nano Structures: Break the Efficiency Bottleneck of Conventional Nanoscale Optoelectronics

Ishtiaque Ahmed Navid[1], Ayush Pandey[1], Yin Min Goh[2], Jonathan Schwartz[2], Robert Hovden[2], and Zetian Mi[1*]

[1]Department of Electrical Engineering and Computer Science, University of Michigan, Ann Arbor, 1301 Beal Avenue, Ann Arbor, MI 48109, USA

[2]Department of Materials Science and Engineering, University of Michigan, Ann Arbor, 2300 Hayward St*, Ann Arbor, MI 48109, USA*

[*] Corresponding author E-mail: ztmi@umich.edu; Phone: 1 734 764 3963

Abstract: Conventional semiconducting nanowire optoelectronic devices generally exhibit low efficiency, due to dominant nonradiative surface recombination. Here, we show that such a critical challenge can be potentially addressed by exploiting semiconducting structures in the deep-nano regime. We have studied the epitaxy and structural and optical characteristics of GaN-based micro-network nanostructures grown on Si wafer. These complex nanostructures have lateral dimensions as small as a few nanometers. Detailed scanning transmission electron microscopy studies suggest that the self-assembled micro-network nanostructures are monocrystalline, despite the porous nature. Significantly, such micro-network nanostructures exhibit ultrabright emission in the visible spectrum. Compared to conventional InGaN nanowire structures with similar surface area, the surface recombination velocity of such deep-nano structures is reduced by nearly two orders of magnitude, which is evidenced by the extremely bright luminescence emission as well as the long carrier lifetime measured under low excitation conditions. This study offers a new path for the design and development of next generation high efficiency nanoscale optoelectronic devices.

In the past two decades, semiconducting nanostructures, *e.g.,* nanowires, have been extensively studied for applications in optoelectronics, including LEDs, lasers, solar cells, and photodetectors.[1] To date, however, it has remained a daunting challenge to achieve high efficiency nanoscale optoelectronic devices. It is generally believed that the underlying challenge is directly related to the enhanced nonradiative surface recombination, due to the large surface area.[2] As an example, while broad area InGaN blue quantum well LEDs can exhibit external quantum efficiency (EQE) >80%,[3] the efficiency decreases by at least one to two orders of magnitude when the device dimensions are reduced to micron, or nanoscale, due to the dominant nonradiative surface recombination.[4] The *efficiency cliff* of optoelectronics, *i.e.,* drastically reduced efficiency when the device sizes are shrunk to the micro or nanoscale, becomes even more severe for III-nitride light emitters in the deep visible (green to red), due to the large lattice mismatch (~11%) between GaN and InN,[5] which not only leads to the formation of extensive defects, disorders, and dislocations, but also significantly reduces the electron-hole wavefunction overlap due to piezo-electric field induced polarization.[6]

The commonly reported semiconducting nanowires for applications in optoelectronics have lateral dimensions on the order of 100 nm, or larger. Glas *et al.*[7] analyzed the critical dimensions for the plastic relaxation of semiconducting nanowires, showing that the critical layer thickness depends strongly on the nanowire diameter. Schematically shown in Figure 1 is the estimated critical layer thickness plotted vs. the nanowire diameter for a heterostructure with lattice mismatch ~4%, corresponding approximately to $In_{0.32}Ga_{0.68}N$ grown on GaN emitting in the green spectrum. The critical layer thickness is ~1 nm for conventional planar heterostructures (shaded grey region in Figure 1), which is increased to ~3 nm for InGaN nanowire structures with diameters ~100 nm (shaded blue region in Figure 1). It is therefore seen that the epitaxy of conventional InGaN/GaN nanowire arrays inevitably leads to certain level of defect formation. The resulting dominant nonradiative (surface) recombination is evident by the extremely short carrier lifetime (sub nanosecond) commonly measured for nanowire structures at room temperature,[8] compared to a few nanoseconds of their planar counterparts, which explains largely the low efficiency of conventional nanowire optoelectronic devices.[9] The critical layer thickness, however, can be potentially increased to an indefinitely large value if the lateral dimensions are further reduced to the deep-nano regime (<40nm), shown as the shaded green region in Figure 1. Indeed, recent studies suggested that strain relaxation was most efficient in InGaN/GaN nanostructures with lateral dimensions <40 nm,[10] consistent with the calculation by Glas *et al.*.[7] Efficient strain relaxation of InGaN nanostructures not only drastically reduces defect densities but also significantly enhances the exciton binding energy due to the increased electron-hole wavefunction overlap.[6c] A nearly 100-fold enhancement in the exciton

oscillator strength was measured in InGaN nanostructures with lateral dimensions <40 nm.[10b] It is therefore envisioned that the *efficiency cliff* of nanoscale optoelectronic devices can be potentially mitigated by developing semiconducting heterostructures in the deep-nano regime. To date, however, the controlled synthesis and optoelectronic properties of such ultrasmall InGaN nanostructures has remained largely unexplored.

Here, we show that the challenges associated with conventional InGaN nanowires can be fundamentally addressed by developing InGaN micro-network nanostructures in the deep nano-regime. We report on the molecular beam epitaxy of InGaN micro-networks grown directly on Si wafer, which can exhibit lateral dimensions as small as 2-5 nm. Detailed structural characterization shows that the self-assembled micro-networks are monocrystalline, despite the complex nanostructures. By controlling the growth conditions, the emission wavelengths can be tuned in the entire visible spectrum. For InGaN micro-network nanostructures emitting in the green wavelength, the emission intensity is nearly two orders of magnitude stronger than conventional InGaN nanowire arrays, due to the significantly reduced defect formation and enhanced exciton oscillator strength. Detailed time-resolved photoluminescence spectroscopy shows that the carrier lifetime is ~6 ns at room temperature. The surface recombination velocity is estimated to be ~150 cms[-1], which is nearly one to two orders of magnitude lower than conventional InGaN nanowire or epilayer structures.[11] This study provides a new generation of nanostructures that are relevant for high efficiency optoelectronic devices in the deep visible.

In this study, Ga(In)N micro-network nanostructures were grown on Si substrate utilizing a Veeco Gen II molecular beam epitaxy (MBE) system equipped with a radio-frequency plasma-assisted nitrogen source (see Experimental Section). Previous studies have shown that, when grown under nitrogen-rich conditions, Ga(In)N nanowires can be readily formed on Si wafer, which are promoted by the initial nucleation of GaN islands on the substrate and their preferential growth along the c-axis driven by energy minimization.[12] Different from conventional nanowire epitaxy, we have employed an ultrathin (approximately sub-nanometer to a few nanometer) AlN buffer layer, schematically shown in Figure 2(a), to precisely control the formation of crystalline GaN micro-network nanostructures with lateral dimensions in the deep-nano regime, *i.e.,* nearly one order of magnitude reduction compared to conventional nanowires grown by MBE.

AlN buffer layer has been commonly used for the epitaxy of III-nitrides on Si wafer,[13] but few studies have paid attention to the effect of the initial AlN nucleation on the subsequent growth and epitaxy process. In this study, the thickness of AlN layer were varied from sub-nm to ~8 nm. Due to the large lattice mismatch (~17%), the epitaxy of a thin AlN layer is described by the Volmer-Weber growth mode,[14] which is characterized by the presence of nanoscale AlN islands, instead of smooth epilayers, on Si substrate. In addition, due to the small Al adatom migration length, these islands are connected, with the presence of extensive voids, forming a nanoscale micro-network-like structure on Si substrate. The atomic force microscopy (AFM) image of an AlN micro-network structure formed on Si wafer is shown in Supporting Information Figure S1. It is found that the micro-network of AlN islands plays a critical role on the subsequent epitaxy of GaN nanostructures. Impingent Ga

6

adatoms migrate through the opening voids. Different from nanowire epitaxy, however, the nucleation sites of GaN are pre-determined by AlN island micro-networks. The nanoscale AlN islands serve as the nucleation sites and promote the coherent epitaxy of GaN, whereas no epitaxy takes place in the opening voids, thereby leading to the formation of unique GaN micro-network nanostructures, schematically shown in Figure 2(a). The crystalline AlN island micro-networks further promote the formation of single crystalline InGaN micro-network nanostructures, to be described next.

Schematically shown in Figure 2(b)-(d) are scanning electron microscopy (SEM) images of GaN nanostructures grown on Si with the use of various AlN buffer layers under otherwise identical conditions (see Experimental Section). Shown in Figure 2(b), without the use of any AlN buffer layer, conventional GaN nanowire arrays are formed directly on Si wafer, which have diameters ~100 nm and are consistent with previous studies. The introduction of a thin (~1 monolayer) AlN buffer layer, however, leads to the mixture of GaN nanowires and micro-networks. The evolution from nanowires to micro-network nanostructures can be clearly observed with gradual increase of the AlN buffer layer thickness. Further increase of the AlN layer thickness suppresses the formation of nanowires and results in GaN micro-network nanostructures. It is also observed that the AlN buffer layer plays a critical role on the morphology and dimension of GaN micro-networks. With increasing AlN buffer layer thickness, there is a gradual decrease of the lateral widths of the micro-network structures to as small as ~5 nm. However, further increasing AlN buffer layer thicknesses beyond 5-10 nm leads to the formation of micro-network structures with larger lateral widths and eventual coalescence. The impact of the AlN buffer layer on the initial as well as the

7

complete growth morphology of GaN nanostructures is also depicted in Supporting Information Figures S2 and S3. We have further investigated the effect of growth parameters on the formation and properties of GaN micro-network nanostructures on an AlN buffer layer with a nominal thickness of ~5 nm. It is observed that the lateral widths of micro-network nanostructures show a decreasing trend with increasing N_2 flow rate and/or increasing growth temperature (see Supporting Information Figures S4 and S5).

The GaN micro-network nanostructures were then utilized as a template for the epitaxy of InGaN nanostructures. N-rich growth conditions were used to promote the epitaxy of InGaN preferentially along the c-axis while suppressing the lateral growth (see Experimental Section). Therefore, InGaN micro-network nanostructures can be readily obtained, shown in Figure 3(a)-(b). Based on the SEM image analysis, it is observed that the average pore size of the structure is ~0.01 square micron with a range of circularity averaging 0.63 and the micro-network lateral dimension averages at 47.18 nm. The details for the distribution for these parameters are presented in the Supporting Information Figure S6(a)-(c). Electron microscopy characterization of the InGaN micro-network nanostructure reveals successful large-scale growth of an In-rich InGaN structure with no phase segregation and high crystallinity. The epitaxial growth of an In-rich InGaN segment on top of a bottom GaN layer is further confirmed through STEM imaging and simultaneous chemical mapping of the micro-network nanostructure structure (Figure 3(c) and Supporting Information Figure S7). Indium distribution in the InGaN segment is unconfined and homogeneous, which suggests large-scale incorporation of In-rich crystal across the entire micro-network nanostructure.

8

As indicated by the sharp diffraction peaks in selected area electron diffraction (SAED) patterns (Figure 3(d)), the InGaN micro-network nanostructures are single crystal and share a common crystallographic axis. The stark crystallinity of the InGaN micro-network defies initial expectations from the specimen's complex mesoscale morphology. Single crystallinity is maintained across microns of material, as shown by the circular aperture selecting the entire micro-network nanostructure in cross-section. Across ~1.75 μm of the micro-network laterally, there is only <0.5 degree rotation of the crystal axis. Crystallinity of the InGaN structure is further verified at atomic resolution with high-angle annular dark field (HAADF) STEM. The atomic structure in Figure 3(e) matches that of the [100] lattice plane of InGaN crystal. The unique single crystalline nature of such complex nanostructure arrays is directly related to the coherent epitaxy of GaN on single crystalline AlN island micro-networks. From our atomic resolution HAADF STEM images, there are no discernible dislocations in the specimen over a 15 nm × 15 nm range, however dislocations could exist beyond the range indicated. The micro-network lateral widths vary from as small as a few nanometers to tens of nanometer, while the height is ~200 nm. The effects of growth parameters on the formation and properties of InGaN micro-network nanostructures were further studied in detail and described in the Supporting Information (Supporting Information Figure S8(a)-(c)).

InGaN micro-network nanostructures grown on Si can exhibit tunable emission across nearly the entire visible spectrum. Shown in Figure 4(a) are the normalized photoluminescence spectra measured at room temperature for InGaN micro-networks with various indium incorporation. It is seen that the emission wavelengths can be controllably tuned from blue

to green, yellow, orange, and red. Figure 4(b) shows the room temperature

photoluminescence spectra of the InGaN micro-network and that of a conventional InGaN

nanowire structure with nearly identical surface area. It is seen that InGaN micro-network

nanostructures exhibit nearly two orders of magnitude enhancement in the luminescence

emission. Shown in Figure 4(c), the extremely bright photoluminescence emission of InGaN

micro-network nanostructures, compared to conventional nanowires, is further confirmed

over a broad range of excitation power. It is worth noting that, given their nearly identical

surface area, the drastically enhanced luminescence intensity cannot be solely explained by

variations in the light extraction efficiency. Instead, the ultra-bright photoluminescence

intensity of the InGaN micro-network nanostructures can be attributed to the significantly

reduced nonradiative surface recombination and enhanced exciton oscillator strength in

such nanoscale structures. Strain relaxation of InGaN/GaN is most significant in

nanostructures with lateral dimensions ~40 nm, or less, as suggested by some recent

studies,[6c, 10] thereby leading to drastically reduced nonradiative (surface) recombination.

Moreover, efficient strain relaxation leads to significantly reduced piezo-electric polarization

fields and therefore enhanced electron-hole wavefunction overlap. As such, the exciton

binding energy increases drastically with reducing lateral dimensions of InGaN

nanostructures. Exciton binding energy value from 70 meV to larger than 100 meV has been

calculated for InGaN nanowall structures with lateral dimensions <40 nm,[6c] which is nearly

five to ten times larger than that in InGaN bulk. Previous studies further suggested that the

exciton oscillator strength of InGaN nanostructures with such small dimensions could be

enhanced by nearly 100-fold, compared to quantum well or conventional nanowire

structures,[10] thereby leading to significantly enhanced quantum efficiency and emission intensity.

Optical properties and carrier dynamics of InGaN micro-network nanostructures were further studied utilizing time-resolved femtosecond laser spectroscopy. The samples were excited with the 400 nm output from the second harmonic of a 80 MHz/70 fs Ti:sapphire laser, focused to a spot of 16 μm diameter. The photoluminescence transient was analyzed using a 0.75 m monochromator and a high-speed single photon counter. The photoluminescence transients for the InGaN micro-network sample measured at different excitation power densities from 2 Wcm^{-2} to 20 k Wcm^{-2} are shown in Figure 5(a). The transients were fitted using a standard stretched exponential decay, and plotted in Figure 5(b), where a relatively long lifetime of over 5 ns was measured for the InGaN micro-network nanostructures at low excitation powers.[15] Such relatively long carrier lifetime is comparable to that of high quality InGaN quantum well structures despite the large surface area, suggesting that nonradiative surface recombination plays a negligible role in the carrier recombination.[15c, 16] This observation is also consistent with the extremely bright photoluminescence emission measured at room temperature and can be well explained by the robust excitonic emission and reduced SRH recombination, which would have the dominant effect on carrier lifetime at low carrier densities. At higher excitation, a decrease in lifetime is observed, which can be attributed to the enhanced radiative recombination and, to some extent, higher order carrier loss terms such as Auger recombination and carrier delocalization.[17] For comparison, significantly shorter carrier lifetime in the range of

11

0.2-0.5 ns have been commonly measured for conventional InGaN nanowire arrays, limited by surface recombination, shown in Figure 5(b).[8]

We further performed excitation power dependent measurements on the InGaN micro-network nanostructures as well as some previously reported spontaneous InGaN nanowire samples [9b] utilizing the same laser source as described above. The photoluminescence signals were analyzed using a 0.75 m monochromator and detected with a UV-enhanced PMT. The relative external quantum efficiency (EQE) at different excitation powers is plotted in Figure 5(c) for both samples. It is seen that the EQE of InGaN micro-network nanostructures is nearly two orders of magnitude higher than that of InGaN nanowire samples, which is consistent with the measurements shown in Figure 4. At higher excitation powers, a clear efficiency droop is observed for the micro-network nanostructures, which is similar to that of conventional high efficiency broad area InGaN light emitters [4a]. Efficiency droop, however, is not seen for the InGaN nanowire sample, due to the dominant nonradiative SRH recombination. To further analyze the data, the generation rate was estimated for different excitation intensities and described in the Supporting Information. (Supporting Information Figure S9).

Under very low excitation conditions, the carrier lifetime is primarily limited by nonradiative surface recombination for nearly strain and defect-free InGaN nanostructures. If neglecting the contribution of bulk recombination to the carrier lifetime, the nonradiative surface recombination lifetime is estimated ~6 ns for micro-network nanostructures, which is nearly

one order of magnitude higher than that of conventional nanowire structures (commonly

measured in the range of 0.2-0.5 ns at room temperature). Therefore, an upper bound of

the surface recombination velocity (S) can be estimated from the following equation,[18]

$$S = \frac{d}{4\tau_{PL}}$$

where d is the lateral width of the nanostructures and τ_{PL} is the carrier lifetime determined

from the TRPL measurements under low excitation conditions. For the micro-network

nanostructures with lateral widths ~30 nm, the surface recombination velocity is calculated

to be ~150 cms^{-1}. For InGaN nanowire samples, based on the commonly measured carrier

lifetime ~0.3 ns and nanowire diameters ~100 nm, the surface recombination velocity is

estimated to be ~10,000 cms^{-1}. It is seen that the strain relaxed InGaN micro-network

nanostructures exhibit a surface recombination velocity that is nearly two orders of

magnitude smaller than conventional nanowires. The drastically reduced surface

recombination, together with the enhanced electron-hole wavefunction overlap and exciton

oscillator strength, can therefore explain the extremely bright luminescence emission of

InGaN micro-network nanostructures.

In summary, we have performed a detailed study of the epitaxy and characterization of

InGaN structures in the deep-nano regime, with lateral dimensions as small as a few nm.

These strain-relaxed nanostructures can exhibit drastically reduced defect formation,

negligible nonradiative surface recombination, as well as significantly enhanced exciton

oscillator strength. Compared to conventional nanowire structures with similar surface area,

the surface recombination velocity of such deep-nano structures is reduced by nearly two orders of magnitude, which is evidenced by the extremely bright luminescence emission as well as the long carrier lifetime measured at room temperature. This study provides a new direction for the design and development of next generation semiconducting nanostructures to break the efficiency bottleneck of nanoscale optoelectronic devices.

Experimental Section

MBE Growth: In this work, the epitaxy of micro-network nanostructures was performed under nitrogen rich conditions using Veeco Gen II radio-frequency plasma-assisted molecular beam epitaxy (MBE) growth system on Si (111) substrate. The Si substrate was cleaned with acetone and methanol and subsequently dipped into 10% buffered hydrofluoric acid prior to loading to eliminate the native oxides. No external metal catalyst was involved for the growth of the micro-network under the nitrogen-rich conditions. The AlN buffer layer growth conditions include a substrate temperature of 810 $^{\circ}$C, Al beam equivalent pressure (BEP) of 2×10^{-8} torr, and N_2 flow rate of 1 sccm. The GaN growth conditions include a substrate temperature 680°C, Ga BEP of 5×10^{-8} torr, and N_2 flow rate 1.5 sccm. Ga BEP of 5×10^{-8} torr, In BEP of 4.5×10^{-8} torr, and 1.5 sccm nitrogen flow rate were used for the InGaN micro-network layer. The initial thin AlN buffer layer was directly grown on Si (111) substrate for up to 5 mins. Then, the bottom GaN layer was grown on top of buffer AlN segment for 1 hour. The top InGaN layer was subsequently grown for 2 hours on top of the GaN layer.

14

Electron Microscopy Methods: HAADF-STEM images with simultaneous STEM-EDS spectroscopic mapping, and SAED patterns were obtained on a Thermo Fisher Talos F200X G2 (200keV, 10.5mrad). The EDS system is equipped with a windowless setup of four silicon drift detectors (SDDs, active area = 4 × 30 mm^2, solid angle = 0.9 srad). Atomic resolution HAADF-STEM images were collected using a JEOL 3100R05 microscope with double Cs aberration corrected STEM (300 keV, 22mrad). Samples for STEM and EDS measurements were prepared in cross-section by mechanical wedge polishing that provides a large and thin area for analyzing samples in the micro-, nano- and atomic scale.

Structural and optical characterization: A He-Cd 325nm laser was used as the excitation source for measuring the room-temperature photoluminescence (PL) of the as-grown InGaN nanowires. The PL emission was detected using a photomultiplier tube (PMT) detector coupled to a SPEX spectrometer. Hitachi SU8000 with an accelerating voltage of 10 kV was used for scanning electron microscopy (SEM) imaging.

Supporting Information

Supporting Information is available from the Wiley Online Library or from the author.

Acknowledgements

Conflict of Interest

15

Some IP related to this work was licensed to NX Fuels, Inc., which was co-founded by Z. Mi.

The University of Michigan and Mi have a financial interest in NX Fuels.

Author Manuscript

References

[1]   a) M. S. Kang, C.-H. Lee, J. B. Park, H. Yoo, G.-C. Yi, *Nano Energy* **2012**, 1, 391; b) C.-H.

        Lee, Y.-J. Kim, Y. J. Hong, S.-R. Jeon, S. Bae, B. H. Hong, G.-C. Yi, *Adv. Mater.* **2011**, 23,

        4614; c) Y. Wang, H. Sun, *Prog. Quantum. Electron.* **2018**, 60, 1; d) J. M. P. Almeida,

        V. Tribuzi, R. D. Fonseca, A. J. G. Otuka, P. H. D. Ferreira, V. R. Mastelaro, P. Brajato,

        A. C. Hernandes, A. Dev, T. Voss, D. S. Correa, C. R. Mendonca, *Opt. Mater.* **2013**, 35,

        2643; e) K. Yu, J. Chen, *Nanoscale Res. Lett.* **2009**, 4, 1; f) E. Y. Chen, C. Milleville, J.

        M. O. Zide, M. F. Doty, J. Zhang, *MRS Energy Sustain.* **2019**, 5, 1; g) J. Park, H. Ryu, T.

        Son, S. Yeon, *Appl. Phys. Express* **2012**, 5, 1; h) L. Sang, J. Hu, R. Zou, Y. Koide, M.

        Liao, *Sci. Rep.* **2013**, 3, 1; i) P. Fan, U. K. Chettiar, L. Cao, F. Afshinmanesh, N. Engheta,

        M. L. Brongersma, *Nat. Photonics* **2012**, 6, 380; j) F.-X. Liang, J.-Z. Wang, Z.-P. Li, L.-B.

        Luo, *Adv. Optical Mater.* **2017**, 5, 1; k) D. Saxena, S. Mokkapati, P. Parkinson, N.

        Jiang, Q. Gao, H. H. Tan, C. Jagadish, *Nat. Photonics* **2013**, 7, 963.

[2]   S. Zhang, A. T. Connie, D. A. Laleyan, H. P. T. Nguyen, Q. Wang, J. Song, I. Shih, Z. Mi,

        IEEE J. Quantum Electron. **2014**, 50, 483.

[3]   a) Y. Narukawa, M. Ichikawa, D. Sanga, M. Sano, T. Mukai, *J. Phys. D: Appl. Phys.*

        2010, 43, 1; b) Y. Narukawa, J. Narita, T. Sakamoto, T. Yamada, H. Narimatsu, M.

        Sano, T. Mukai, *phys. stat. sol. (a)* **2007**, 204, 2087.

[4]   a) T. Kohno, Y. Sudo, M. Yamauchi, K. Mitsui, H. Kudo, H. Okagawa, Y. Yamada, *Jpn. J.*

        Appl. Phys. **2012**, 51, 1; b) A. Y. Polyakov, N. B. Smirnov, A. V. Govorkov, H. Amano, S.

        J. Pearton, I.-H. Lee, Q. Sun, J. Han, S. Y. Karpov, *Appl. Phys. Lett.* **2011**, 98, 1; c) X.

        Liu, Y. Wu, Y. Malhotra, Y. Sun, Z. Mi, *Appl. Phys. Lett.* **2020**, 117, 1.

[5]   a) S. De, A. Layek, S. Bhattacharya, D. K. Das, A. Kadir, A. Bhattacharya, S. Dhar, A. Chowdhury, *Appl. Phys. Lett.* **2012**, 101, 1; b) J. W. Robinson, J. H. Rice, K. H. Lee, J. H. Na, R. A. Taylor, D. G. Hasko, R. A. Oliver, M. J. Kappers, C. J. Humphreys, G. A. D. Briggs, *Appl. Phys. Lett.* **2005**, 86, 1; c) J.-H. Ryou, P. D. Yoder, J. Liu, Z. Lochner, H. Kim, S. Choi, H. J. Kim, R. D. Dupuis, *IEEE J. Sel. Top. Quantum Electron.* **2009**, 15, 1080.

[6]   a) A. E. Romanov, T. J. Baker, S. Nakamura, J. S. Speck, *J. Appl. Phys.* **2006**, 100, 1; b) T. Takeuchi, H. Amano, I. Akasaki, *Jpn. J. Appl. Phys.* **2000**, 39, 413; c) S. Sankaranarayanan, S. Chouksey, P. Saha, V. Pendem, A. Udai, T. Aggarwal, S. Ganguly, D. Saha, *Sci. Rep.* **2018**, 8, 1.

[7]   F. Glas, *Phys. Rev. B* **2006**, 74, 1.

[8]   a) M. Biswas, R. Kumar, A. Chatterjee, Y. Wu, Z. Mi, P. Bhattacharya, S. K. Pal, S. Chakrabarti, *J. Lumin.* **2020**, 222, 1; b) S. Deshpande, T. Frost, L. Yan, S. Jahangir, A. Hazari, X. Liu, J. Mirecki-Millunchick, Z. Mi, P. Bhattacharya, *Nano Lett.* **2015**, 15, 1647; c) W. Guo, M. Zhang, A. Banerjee, P. Bhattacharya, *Nano Lett.* **2010**, 10, 3355; d) S. Jahangir, A. Banerjee, P. Bhattacharya, *Phys. Status Solidi C* **2013**, 10, 812; e) C. Zhao, T. K. Ng, R. T. ElAfandy, A. Prabaswara, G. B. Consiglio, I. A. Ajia, I. S. Roqan, B. Janjua, C. Shen, J. Eid, A. Y. Alyamani, M. M. El-Desouki, B. S. Ooi, *Nano Lett.* **2016**, 16, 4616.

[9]   a) Y. Zhang, J. Wu, M. Aagesen, H. Liu, *J. Phys. D: Appl. Phys.* **2015**, 48, 1; b) S. Zhao, H. P. T. Nguyen, M. G. Kibria, Z. Mi, *Prog. Quantum. Electron.* **2015**, 44, 14.

[10]   a) Y. Kawakami, A. Kaneta, L. Su, Y. Zhu, K. Okamoto, M. Funato, A. Kikuchi, K.

Kishino, *J. Appl. Phys.* **2010**, 107, 1; b) L. Zhang, L.-K. Lee, C.-H. Teng, T. A. Hill, P.-C.

Ku, H. Deng, *Appl. Phys. Lett.* **2014**, 104, 1.

[11]   a) R. Aleksiejūnas, M. Sūdžius, T. Malinauskas, J. Vaitkus, K. Jarašiūnas, S. Sakai,

Applied physics letters **2003**, 83, 1157; b) J. B. Schlager, K. A. Bertness, P. T.

Blanchard, L. H. Robins, A. Roshko, N. A. Sanford, *Journal of applied physics* **2008**,

103, 124309; c) V. Ramesh, A. Kikuchi, K. Kishino, M. Funato, Y. Kawakami, *Journal of

Applied Physics* **2010**, 107, 114303; d) K. A. Bulashevich, S. Y. Karpov, *physica status

solidi (RRL)–Rapid Research Letters* **2016**, 10, 480; e) M. Boroditsky, I. Gontijo, M.

Jackson, R. Vrijen, E. Yablonovitch, T. Krauss, C.-C. Cheng, A. Scherer, R. Bhat, M.

Krames, *Journal of Applied Physics* **2000**, 87, 3497; f) H. Kitagawa, T. Suto, M. Fujita,

Y. Tanaka, T. Asano, S. Noda, *Applied physics express* **2008**, 1, 032004; g) P. Ščajev,

K. Jarašiūnas, S. Okur, Ü. Özgür, H. Morkoç, *Journal of Applied Physics* **2012**, 111,

023702.

[12]   a) R. Calarco, R. J. Meijers, R. K. Debnath, T. Stoica, E. Sutter, H. Luth, *Nano Lett.*

2007, 7, 2248; b) R. K. Debnath, R. Meijers, T. Richter, T. Stoica, R. Calarco, H. Lüth,

Appl. Phys. Lett. **2007**, 90, 1.

[13]   a) Y. Tamura, K. Hane, *Nanoscale Res. Lett.* **2015**, 10, 1; b) A. Zhong, P. Fan, Y. Zhong,

D. Zhang, F. Li, J. Luo, Y. Xie, K. Hane, *Nanoscale Res. Lett.* **2018**, 13, 1; c) A. Zhong, K.

Hane, *Jpn. J. Appl. Phys.* **2013**, 52, 1.

[14]   a) M. M. R. Evans, J. C. Glueckstein, J. Nogami, *Phys. Rev. B* **1996**, 53, 4000; b) C.

Friesen, S. C. Seel, C. V. Thompson, *J. Appl. Phys.* **2004**, 95, 1011; c) V. M. Kaganer, B.

Jenichen, R. Shayduk, W. Braun, H. Riechert, *Phys. Rev. Lett.* **2009**, 102, 1; d) H. Z. Yu, C. V. Thompson, *Acta Mater.* **2014**, 67, 189.

[15]   a) A. Aiello, A. Pandey, A. Bhattacharya, J. Gim, X. Liu, D. A. Laleyan, R. Hovden, Z. Mi, P. Bhattacharya, *J. Cryst. Growth* **2019**, 508, 66; b) A. Aiello, Y. Wu, A. Pandey, P. Wang, W. Lee, D. Bayerl, N. Sanders, Z. Deng, J. Gim, K. Sun, R. Hovden, E. Kioupakis, Z. Mi, P. Bhattacharya, *Nano Lett.* **2019**, 19, 7852; c) M. Pophristic, F. H. Long, C. Tran, I. T. Ferguson, J. R. F. Karlicek, *Appl. Phys. Lett.* **1998**, 73, 3550.

[16]   a) M. Pophristic, F. H. Long, C. Tran, I. T. Ferguson, J. R. F. Karlicek, *J. Appl. Phys.* **1999**, 86, 1114; b) Y. C. Shen, G. O. Mueller, S. Watanabe, N. F. Gardner, A. Munkholm, M. R. Krames, *Appl. Phys. Lett.* **2007**, 91, 1.

[17]   a) T. Lin, H. C. Kuo, X. D. Jiang, Z. C. Feng, *Nanoscale Res. Lett.* **2017**, 12, 1; b) T. Lin, Z. R. Qiu, J.-R. Yang, L. Ding, Y. h. Gao, Z. C. Feng, *Mat. Lett.* **2016**, 173, 170; c) E. F. Schubert, *Light-Emitting Diodes*, Cambridge University Press, **2006**.

[18]   a) C.-C. Chang, C.-Y. Chi, M. Yao, N. Huang, C.-C. Chen, J. Theiss, A. W. Bushmaker, S. LaLumondiere, T.-W. Yeh, M. L. Povinelli, C. Zhou, P. D. Dapkus, S. B. Cronin, *Nano Lett.* **2012**, 12, 4484; b) Y. Dan, K. Seo, K. Takei, J. H. Meza, A. Javey, K. B. Crozier, *Nano Lett.* **2011**, 11, 2527; c) A. Higuera-Rodriguez, B. Romeira, S. Birindelli, L. E. Black, E. Smalbrugge, P. J. v. Veldhoven, W. M. M. Kessels, M. K. Smit, A. Fiore, *Nano Lett.* **2017**, 17, 2627.
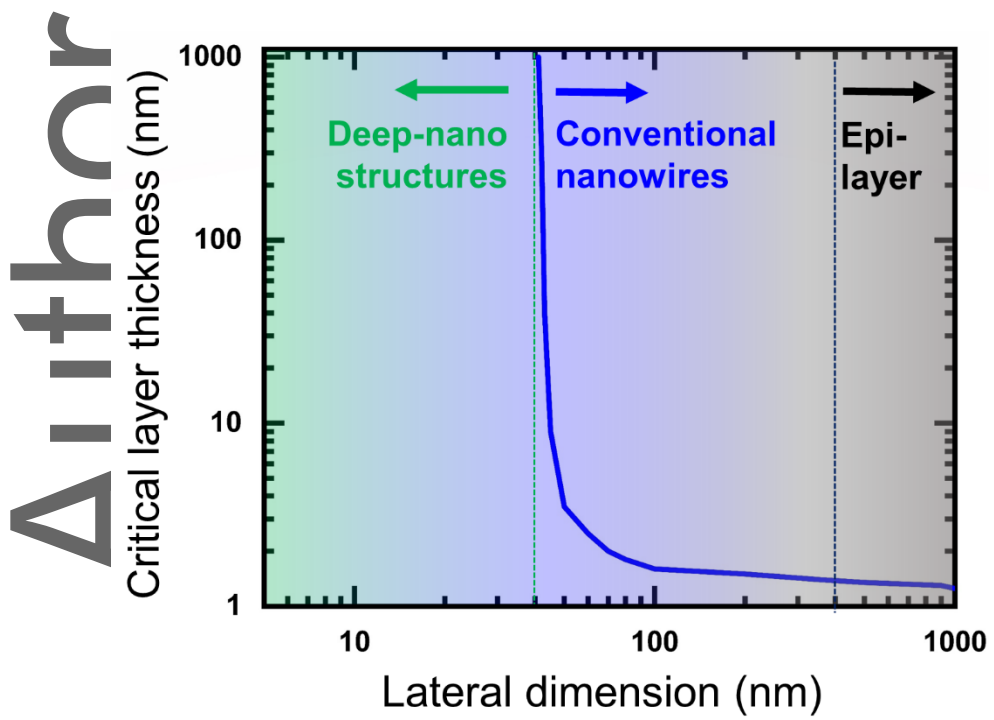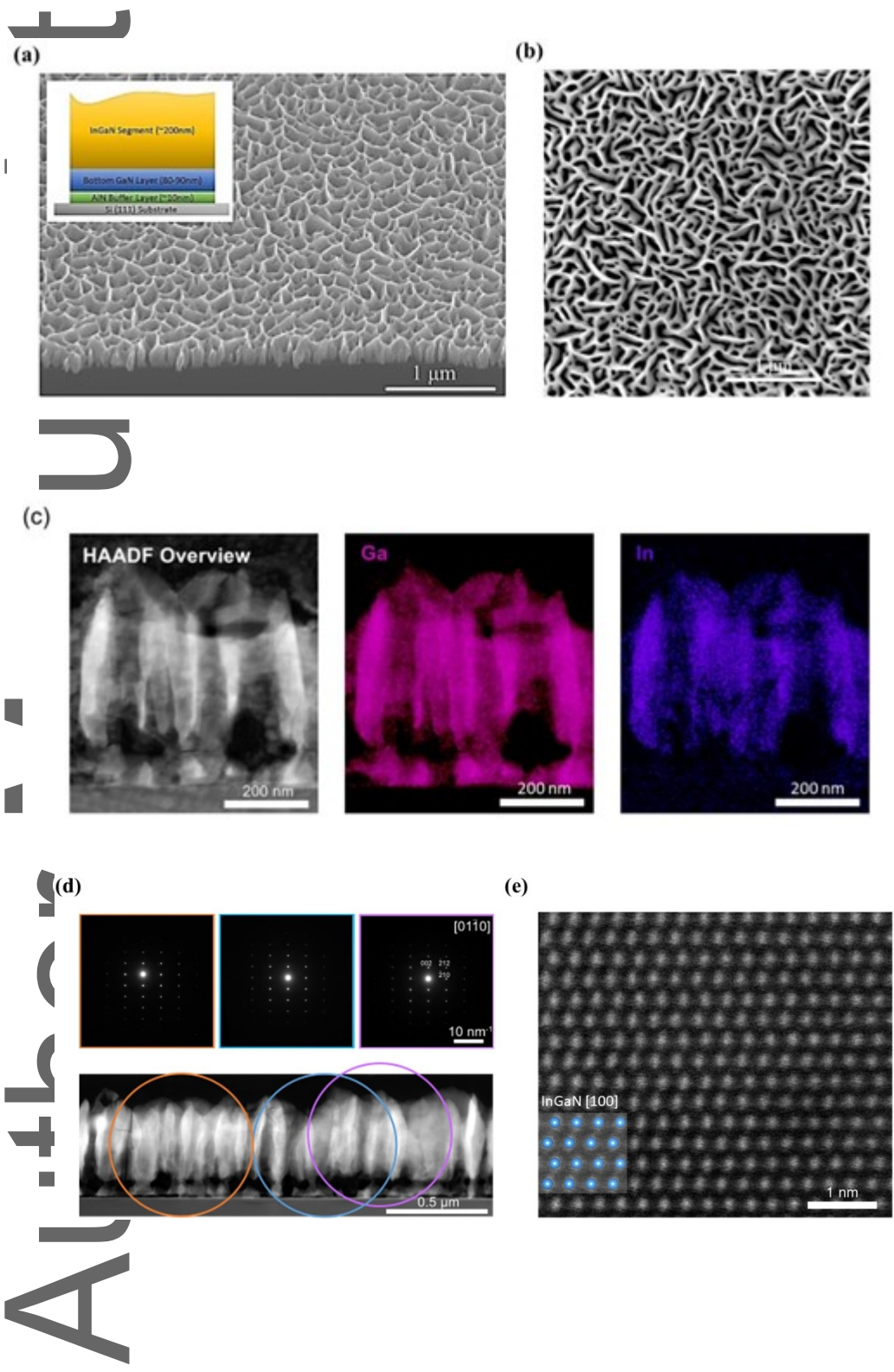
Figure 1. Schematic illustration of the critical thickness variation of a lattice-mismatched heterostructure as a function of the lateral dimension. Blue curve: variation of the critical layer thickness for a misfitting layer (misfit ~4%) growing on top of a nanowire as a function of the nanowire radius (Adapted from Glas *et al.* [7]). It is seen that in the deep-nano regime, the critical layer thickness can be infinitely large.
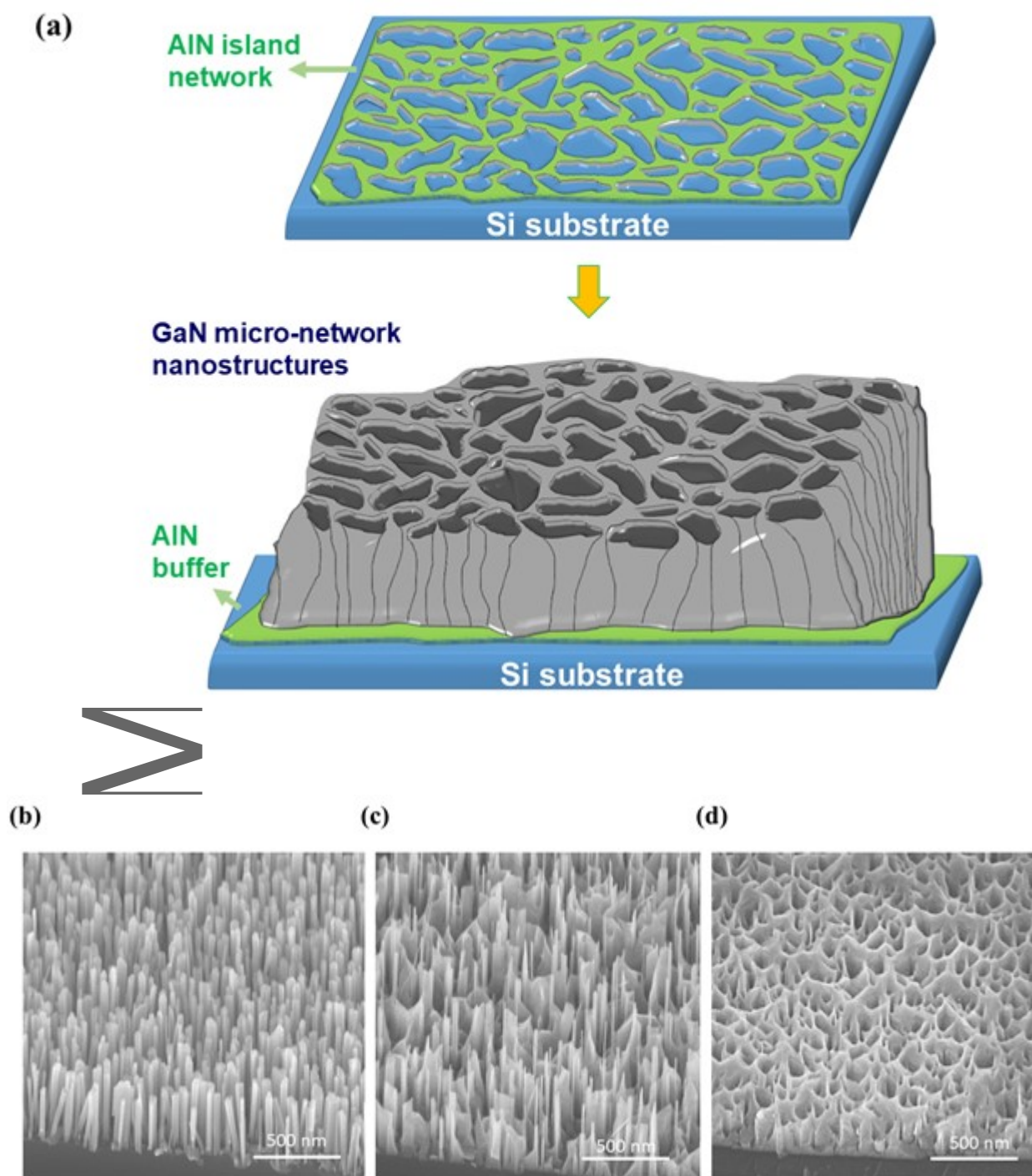
Figure 2. (a) Schematic representation GaN micro-network nanostructure grown on Si substrate with AlN buffer layer. (b-d) SEM images of GaN nanostructures grown on Si. (b) Nanowire arrays are formed on Si in the absence of any AlN buffer layer. (c) A mixture of nanowires and micro-network nanostructures are formed on Si with the use of ~1 ML thick AlN buffer layer. (d) Formation of GaN micro-network nanostructures on Si with the use of ~8 nm thick AlN buffer layer.

(a)

InGaN Segment (~200nm)

Bottom GaN Layer (80-90nm)

AlN Buffer Layer (~200nm)

Si (111) Substrate

1 µm

(b)

(c)

HAADF Overview

Ga

In

200 nm

200 nm

200 nm

(d)

[0110]

002 212
210

10 nm⁻¹

0.5 µm

(e)

InGaN [100]

1 nm

24

Figure 3. (a) SEM image of as-grown InGaN micro-network nanostructures on Si (111) substrate at 45° tilt angle. Inset: schematic of the layer structure. (b) Top view SEM image of as-grown InGaN micro-network nanostructures. (c) High-angle annular dark field (HAADF) STEM image of cross-sectional InGaN micro-network nanostructures with energy-dispersive X-ray (EDS) elemental mapping of Ga and In atoms. (d) Selected area electron diffraction (SAED) across ~2.5 μm of micro-network nanostructure in cross section. Imaging regions corresponding to each SAED pattern are marked by circular apertures with matching colors. Single-crystallinity is maintained over the entire range (~2.5 μm) with only 0.5° crystal rotation over a distance of 1.75 μm. (e) Atomic resolution HAADF-STEM confirms that the specimen is highly crystalline and consistent with the InGaN [100] lattice plane.
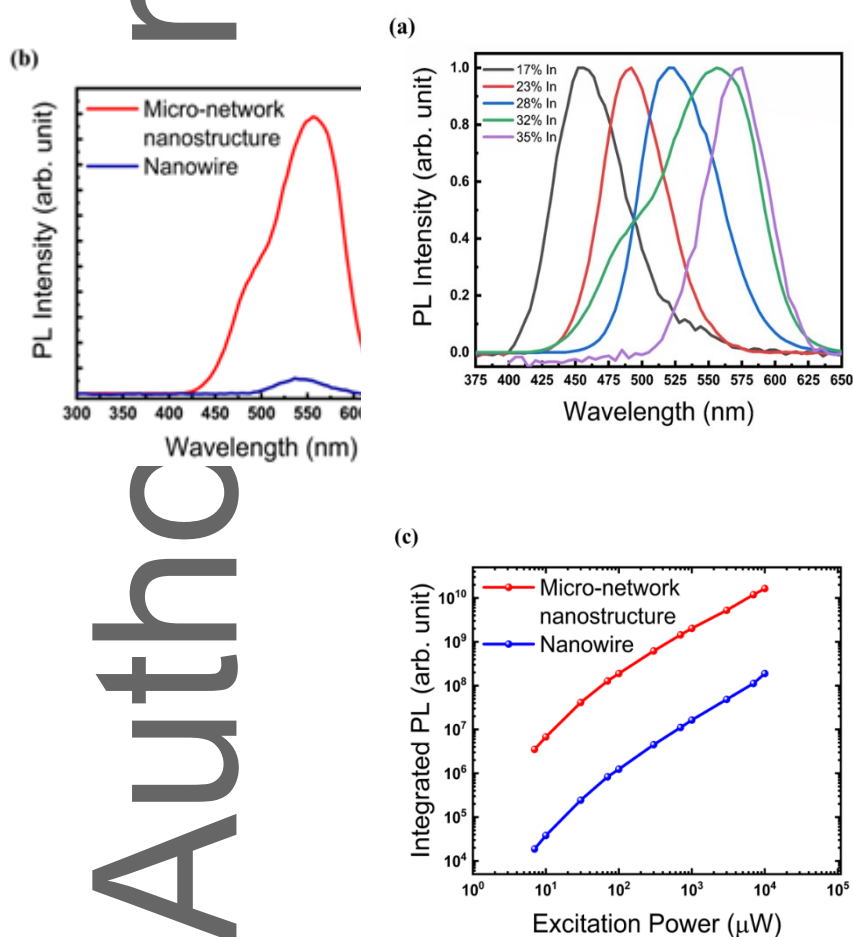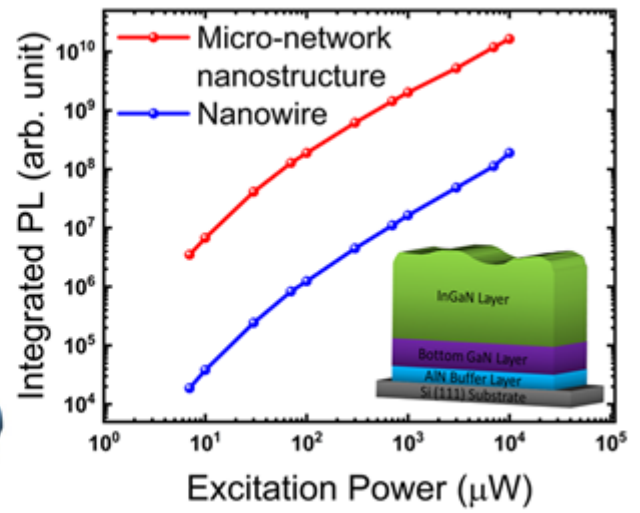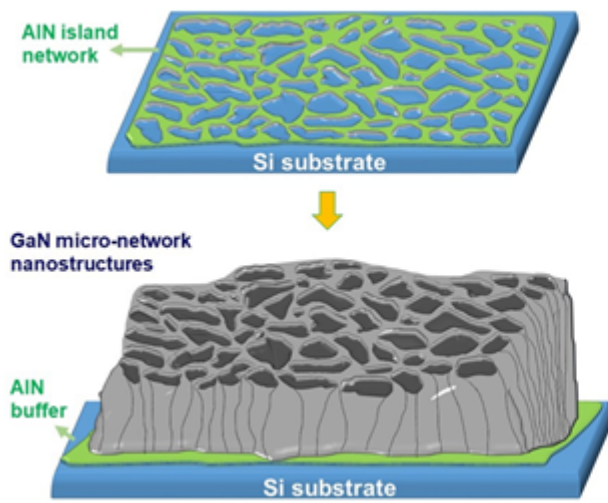
Figure 4. (a) Normalized room-temperature photoluminescence (PL) spectra for InGaN micro-network nanostructures, showing tunable emission in the entire visible spectrum. (b) Photoluminescence spectra of the InGaN micro-network sample and conventional InGaN nanowire structures with similar surface area, showing nearly two orders of magnitude enhancement of the luminescence emission. (c) Variations of the integrated PL intensity with excitation power for InGaN micro-network and nanowire structures measured at room temperature.
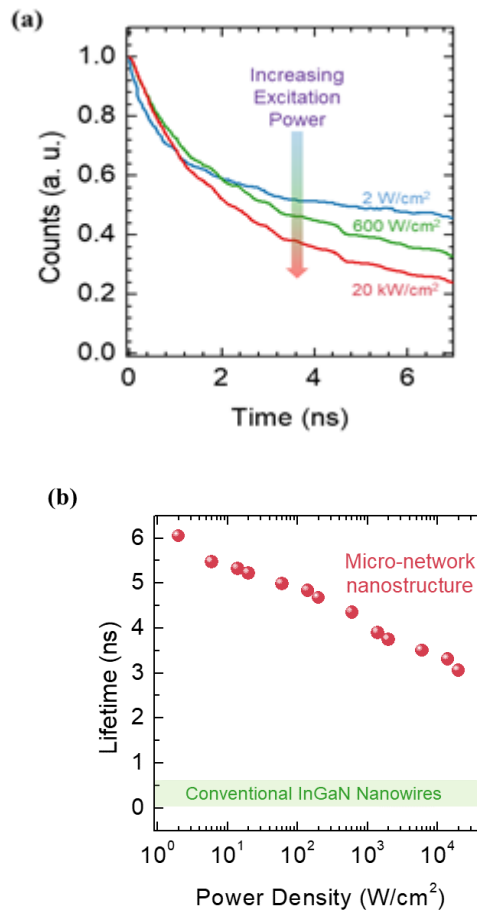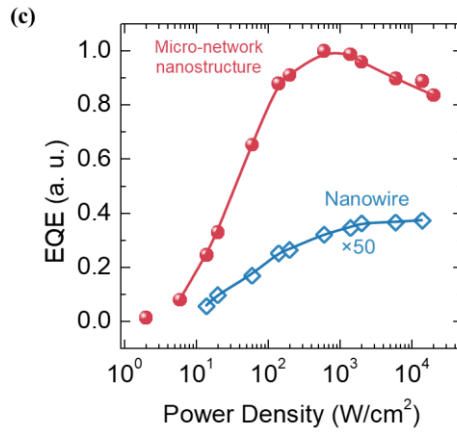
Figure 5. (a) TRPL for InGaN micro-network nanostructures measured at different excitation powers. (b) Carrier lifetime versus excitation power density of the InGaN micro-network nanostructures and InGaN nanowires at room temperature. (c) EQE variation as a function of power density for InGaN micro-network nanostructures and InGaN nanowires, showing nearly two orders of magnitude enhancement of luminescence emission efficiency of micro-network nanostructures, compared to conventional nanowires.

A detailed study of the epitaxy and characterization of GaN/InGaN micro-network structures in the deep-nano regime has been performed. These strain-relaxed micro-network nanostructures show negligible nonradiative surface recombination and remarkable enhancement in exciton oscillator strength. As such, they exhibit significantly reduced surface recombination velocity compared to nanowires evidenced by drastically high photoluminescence intensity and long carrier lifetime at room temperature.

Author Manus